

Optical properties of single crystal Nd³⁺-doped Bi₄Ge₃O₁₂: Laser transitions at room and low temperature

G. A. Kumar* and R. E. Riman

Department of Material Science & Engineering, Rutgers—The State University of New Jersey, 607 Taylor Road, Piscataway,
New Jersey 08854-8065, USA

Alexander A. Kaminskii

Institute of Crystallography, Russian Academy of Sciences, Crystal Laser Physics Laboratory, Leninskii pr. 59, Moscow 119333, Russia

R. Praveena and C. K. Jayasankar

Department of Physics, Sri Venkateswara University, Tirupati 517 502, India

I. K. Bae, S. C. Chae, and Y. N. Jang

Minerals and Materials Processing Division, Korea Institute of Geoscience and Mineral Resources (KIGAM), 30 Kajungdong, Yusunggu
Daejeoun, Korea

(Received 30 November 2005; revised manuscript received 21 April 2006; published 31 July 2006)

A Nd³⁺-doped Bi₄Ge₃O₁₂ (BGO) single crystal was grown by the modified Czochralski method. Using the 4*f*-energy matrix diagonalization procedure various interaction parameters viz. Slater-Condon (F^2 , F^4 , and F^6), spin-orbit (ξ), two body interaction (α , β , and γ), Judd parameter (T^2 , T^3 , T^4 , T^6 , T^7 , and T^8), spin-other-orbit parameters (M^0 , M^2 , and M^4) and electrostatically correlated spin-orbit interaction parameters (P^2 , P^4 , and P^6), and the crystal-field parameters (B_q^k) were evaluated. The crystal-field analysis has also been carried out for Nd³⁺:Bi₄Si₃O₁₂, Eu³⁺:BGO, and Er³⁺:BGO systems. The potential of a BGO crystal as a laser crystal for 1064.4 and 1341.8 nm was established by quantitative analysis of the absorption, emission spectrum, and fluorescence decay characteristics. Judd-Ofelt parametrization was employed to compute the radiative spectral parameters such as radiative transition probabilities, fluorescence branching ratios, stimulated emission cross sections, and quantum efficiencies of the observed bands in the fluorescence spectrum. Using the measured radiative properties, 100% quantum efficiency was obtained for the principal emission band at 1064.4 nm with an effective stimulated emission cross section of 1.34×10^{-19} cm². The high stimulated emission cross section, fluorescence branching ratio, and quantum efficiency indicate that the Nd³⁺-doped BGO crystal can be a suitable host for 1064.4 and 1341.8 nm emission wavelengths in *Q*-switched laser applications.

DOI: 10.1103/PhysRevB.74.014306

PACS number(s): 71.20.Eh, 71.35.Cc, 71.70.Ch, 71.70.Ej

I. INTRODUCTION

With the introduction of widely tunable diode laser sources, diode-pumped solid-state lasers are becoming increasingly important. A plethora of work has been done on the spectroscopic and laser characteristics of a large variety of crystalline materials over the past decades.¹ Bismuth germanate, Bi₄Ge₃O₁₂ (BGO) has become an important material because of its technological applications especially in x-ray, γ -ray, and high energy particle detectors.²⁻⁴ BGO also has other very interesting physical properties, which include electro-optical, nonlinear, and acousto-optical applications among others.⁵

In this paper, we analyze the energy level structures of Nd³⁺:BGO, Nd³⁺:BSO (Bi₄Si₃O₁₂), Eu³⁺:BGO, and Er³⁺:BGO single crystals grown by the Czochralski method and obtained the values of various spectroscopic parameters viz. Slater-Condon (F^k , $k=2, 4$, and 6), spin-orbit (ξ), two body interaction (α , β , and γ), Judd parameter (T^i , $i=2, 3, 4, 6, 7$, and 8), spin-other-orbit parameters (M^j , $j=0, 2$, and 4) and electrostatically correlated spin-orbit interaction parameters (P^k , $k=2, 4$, and 6), and the crystal-field parameters B_q^k using the 4*f*-energy matrix diagonalization procedure. Further, the Judd-Ofelt theory has been used to quantitatively

estimate the transition probabilities, fluorescence branching ratios, stimulated emission cross sections, and quantum efficiencies of various emission bands and corresponding Stark levels observed in the emission spectrum for Nd³⁺-doped BGO.

II. EXPERIMENT

A. Crystal structure

BGO crystal has the space group $\bar{I}43d$ and the local site symmetry of the Nd³⁺ ion in BGO belongs to $\bar{4}3m$ point symmetry groups. The unit cell contains four formula units, i.e., 76 atoms. The lattice parameters are $a=b=c=1.0518 \pm 0.001$ nm.⁶ In cubic BGO, the Ge ions are tetrahedrally coordinated by four O²⁻ ions, while Bi³⁺ ions are octahedrally coordinated by six triagonally-distorted O²⁻ ions. Nd³⁺ ions substitute for bismuth.^{7,8} Thus it is possible that the trigonal distortion will split the Nd³⁺ electronic energy levels into multiple Stark levels. Bi³⁺ ions occupy a special 16-fold position in the unit cell (Fig. 1) with the following atomic coordinates:

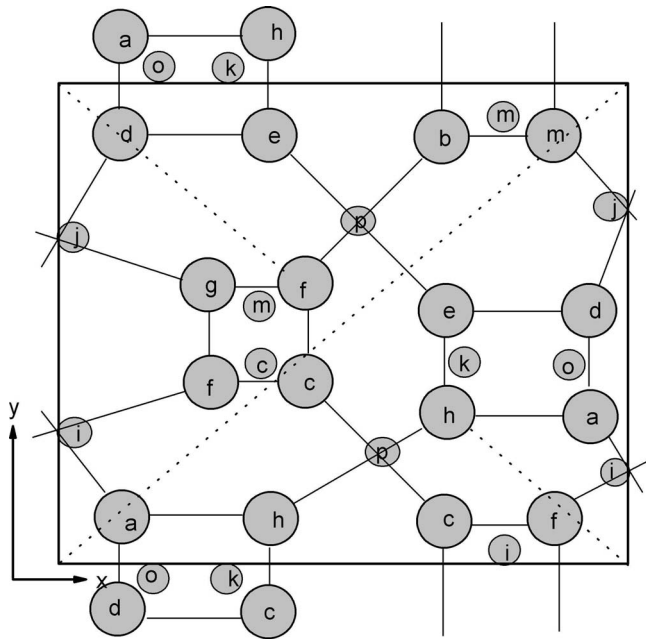


FIG. 1. Cation positions in the unit cell of the BGO crystal lattice. Large circles, Bi ions; small circles, Ge ions; z coordinates: a, 0.0857; b, 0.1643; c, 0.3357; d, 0.4143; e, 0.05857; f, 0.6643; g, 0.8357; h, 0.9143; i, 0.0; j, 0.125; k, 0.25; l, 0.375; m, 0.5; n, 0.625; o, 0.75; p, 0.875.

$$\begin{array}{cccccc}
 u & u & u & u + \frac{1}{4} & u + \frac{1}{4} & u + \frac{1}{4}, \\
 \frac{1}{2} - u & u & \bar{u} & \bar{u} - \frac{1}{4} & \bar{u} - \frac{1}{4} & u + \frac{1}{4}, \\
 \bar{u} & \frac{1}{2} - u & u & u + \frac{1}{4} & \bar{u} - \frac{1}{4} & \bar{u} + \frac{1}{4}, \\
 u & \bar{u} & \frac{1}{2} - u & \bar{u} + \frac{1}{4} & u + \frac{1}{4} & \bar{u} - \frac{1}{4},
 \end{array}$$

and the same set once more with the addition of $\frac{1}{2}$ to each coordinate ($x + \frac{1}{2}$, $y + \frac{1}{2}$, and $z + \frac{1}{2}$); $u = 0.0857 \pm 0.002$.⁹ The Ge atoms occupy a special 12-fold position with the generating coordinates $\frac{3}{8}$, 0, and $\frac{1}{4}$. The 48 oxygen atoms occupy a general position x, y, z with the following generating parameters: $x = 0.0607 \pm 0.002$, $y = 0.1335 \pm 0.004$, and $z = 0.2875 \pm 0.002$. The shortest Bi-Bi distance in BGO is measured to be 0.388 nm.

B. Crystal growth

Nd³⁺-doped BGO was grown by means of the Czochralski method using resistance heating. We used the same resistance-heating furnace, that had been employed previously for Er³⁺-doped CaF₂.¹⁰ The furnace consisted of six *U*-type Super Kanthal heating elements placed radially in order to achieve balanced thermal conditions with a maximum attainable temperature of 1973 K. Two Pt-Pt-10% Rh thermocouples were used with the system; the one for controlling temperature was placed close to the heating elements and the other was located in the bottom of the crucible in order to measure the melt temperature of the sample. The internal size of the furnace was 110 mm in height and 110 mm in diameter. Both thermocouples were of Pt-Pt-10% Rh type. A frequency-weighting sensor, developed

by the Korea Institute of Geology, Mining, and Materials (KIGAM) (Ref. 11) provided feedback control for determining the pulling rate of the crystal.

Bi₂O₃ (99.99%, CERAK Co.), GeO₂ (99.99%, CERAC Co., Milwaukee, WI), and Nd₂O₃ (99.99%, CERAC Co.) were used as raw materials. A platinum crucible of 50 mm in height and 40 mm in diameter was used. The starting materials were weighed, mixed, sintered, and charged into a 50 × 40 mm crucible and a Nd:Bi₄Ge₃O₁₂ crystal was grown by the Czochralski method and then cooled slowly. From necking to shouldering, manual temperature control was employed based on data from the sensor, i.e., diameter, weight, etc. A steady pulling rate was initiated once the predetermined desired diameter had been reached.

A pure BGO crystal was used as a seed crystal. It was grown by KIGAM, also by the Czochralski method. The dominant crystal growth direction was $\langle 110 \rangle$. The optimum conditions of Nd³⁺-doped crystal growth corresponded to pulling rates of 2–0.8 mm/h, rotation rates of 45–15 rpm, and an O₂ gas atmosphere. The dimensions of the crystal obtained were 20 × 15 × 5 mm.

The room temperature and low temperature (77 K) optical absorption spectra were recorded using a double beam spectrophotometer (Perkin Elmer Lambda 9, Wellesley, MA) in the UV-VIS-NIR range. Luminescence spectra were recorded by exciting the crystal by the 800 nm band of a Ti:S ring laser (model 899-01, Coherent Inc, Santa Clara, CA). The infrared emission was collected, focused, and dispersed using a 1 m double monochromator (Triax 550, Jobin Yvon, Edison, NJ). The signals were detected with a thermoelectrically cooled In_xGa_{1-x}As detector. A lock-in amplifier (Stanford Research System, model SR850 DSP, CA) amplified the output signal of the In_xGa_{1-x}As (EO systems, Phoenixville, PA) detector. The spectrometer and the detection system were interfaced by a data acquisition system that was controlled with GRAMS 32 (Galactic Corp, Salem, NH) commercial software. Luminescence decay times were measured at the excitation wavelength 800 nm by modulating the laser at 400 Hz and the signal was detected using a digital storage oscilloscope (model 54520A, 500 MHz, Hewlett Packard, Palo Alto, CA).

C. Energy level calculations and crystal-field analysis

The energy level calculations were carried out as described elsewhere.^{12,13} The model Hamiltonian that was used to study the energy level structure of rare earth ions is written as¹²⁻¹⁴

$$\hat{H} = \hat{H}_A + \hat{H}_{CF} \quad (1)$$

where \hat{H}_A is defined to incorporate the isotropic parts of \hat{H} (including the spherically symmetric part of the 4f-electron-crystal-field interactions) and \hat{H}_{CF} is defined to represent the nonspherically symmetric components of the even-parity crystal-field (CF). Further details are given elsewhere.¹²⁻¹⁴

The \hat{H}_A is referred to as the atomic Hamiltonian and is characterized by a set of 20 free-ion parameters¹²⁻¹⁴ that in-

clude Slater-Condon (F^k), spin-orbit (ξ), two body interaction (α , β , and γ), Judd parameters (T^i), spin-other-orbit parameters (M^i), and electrostatically correlated spin-orbit interaction parameters (P^k). The number of parameters for \hat{H}_{CF} in Eq. (1) depends on the symmetry selection rules for the point symmetry at the rare earth ion site in the crystal. For Bi₄Ge₃O₁₂ and Bi₄Si₃O₁₂ (BSO) crystals, it was assumed that the rare earth ions occupy Bi³⁺ sites with C_3 point symmetry.^{15–19} Therefore, the CF Hamiltonian for C_3 point symmetry may be represented as follows:^{14,20}

$$H_{CF} = B_0^2 C_0^2 + B_0^4 C_0^4 + B_3^4 (C_3^4 - C_{-3}^4) + iS_3^4 (C_3^4 + C_{-3}^4) \\ + B_0^6 C_0^6 + B_3^6 (C_3^6 - C_{-3}^6) + iS_3^6 (C_3^6 + C_{-3}^6) \\ + B_6^6 (C_6^6 + C_{-6}^6) + iS_6^6 (C_6^6 - C_{-6}^6). \quad (2)$$

The matrix elements of C_q^k in Eq. (2) which are spherical tensor harmonics can be calculated theoretically,¹⁴ whereas the real B_q^k and imaginary S_q^k CF parameters can be either calculated theoretically or fitted with the experimentally observed energy level scheme.^{12–14} The computer program developed by Reid²¹ was used to treat the crystal-field parameters as variable parameters in fitting the eigenvalues of the Hamiltonian matrix to the observed energy level scheme.

However, in low symmetries, with many complex CF parameters, least squares fits are often unstable because the energy levels may be relatively insensitive to the (crystal-field) phase factor.²² Also, the more parameters that are involved, the more spurious solutions result, particularly when the experimental data are limited. In order to derive more meaningful parameters, the following approaches have been used to optimize as well as to reduce the number of CF parameters for fitting the experimental data:

(1) approximate the known actual point symmetry group by a higher point symmetry. For example, the use of C_{2v} instead of C_2 symmetry for lanthanide ions in LaF₃²³ and the use of D_{2d} instead of S_4 symmetry for lanthanide ions in LiYF₄ and LiBiF₄.²⁴

(2) rotate the x , y coordinates around the crystallographic C_3 axis to set one of the three imaginary terms S_3^4 , S_3^6 , and S_6^6 to zero. This rotation does not affect the “length” of the complex CF parameter, so if you set S_3^4 equal to zero, the new B_3^4 parameter will equal the “length” of the complex parameter $[(B_3^4 + S_3^4)^{1/2}]$.

(3) descending symmetry procedure, e.g., C_{4v} reduce to C_{2v} for the rare earth oxysulfate series.²⁵ Rudowicz,²⁶ Rudowicz, and Qin,^{20,27,28} as well as Burdick and Reid²² have carried out extensive work on various aspects and importance of crystal-field parameters and crystal-field Hamiltonian along with reliability and compatibility of real and imaginary crystal-field parameters, particularly for low symmetry systems. Therefore, for complete details of calculations and trends of CF parameters for trivalent lanthanide ions, we refer the reader to Refs. 20–22 and 26–28.

In view of the above facts in the present work, the CF parameters have been optimized using an approximate C_{3v} point symmetry [imaginary S_q^k crystal-field parameters given in Eq. (2) vanish] instead of the actual C_3 symmetry. Thus, a total of 20 free-ion parameters and 6 CF parameters may be

TABLE I. Spectroscopic and crystal-field parameters for Nd³⁺-doped BGO, Nd³⁺-doped BSO, Eu³⁺-doped BGO, and Er³⁺-doped BGO systems. All values are in cm⁻¹.

Parameters	Nd:BGO	Nd:BSO	Eu:BGO	Er:BGO
E_{AVG}	24971	24968	64576	35481
F^2	79338	[79338] ^a	84719	98507
F^4	44507	[44507]	58221	70524
F^6	46394	[46394]	42685	51741
ξ	869	[869]	1341	2345
α	20.70	[20.70]	16.62	23.42
β	-598	[-598]	-678	-876
γ	1524	[1524]	1804	1856
T^2	[380]	[380]	[370]	[286]
T^3	[39]	[39]	[40]	[48]
T^4	[62]	[62]	[40]	[14]
T^6	[-290]	[-290]	[-330]	[-324]
T^7	[352]	[352]	[380]	[172]
T^8	[363]	[363]	[370]	[323]
M^0	[1.83]	[1.83]	[2.38]	[3.56]
P^2	[256]	[256]	[245]	[381]
B_0^2	836	824	526	391
B_0^4	63	-169	154	-303
B_3^4	±2220	±2067	±1491	±1909
B_0^6	147	335	200	460
B_3^6	±90	±42	±94	±64
B_6^6	423	468	-275	188
N^b	55	27	35	31
σ^c	±22	±41	±22	±16
S^d	305	575	754	539

^aThe parameter values in square brackets were held fixed in the fitting calculations.

^b N refers to the number of levels used in the fit.

^c σ refers to the rms deviation between experimental and calculated energies.

^d S refers to the crystal-field strength.

used in the fitting approach to the $4f^m$ -electronic structure problem.²¹ The starting parameter values are crucial for energy level calculations that result with a small root mean square (rms) deviation (σ) between the experimental and calculated energy levels as well as consistent parameters values. Systematic CF analysis reveals that slight changes in the free-ion parameters by changing the host does not significantly affect the behavior of CF parameters. Further, in some cases crystal-field calculations are carried out by using the free-ion parameters of aquo-ions for Ln³⁺:Y₂O₃ energy level analysis.²⁹ Ln³⁺:LaCl₃ free-ion parameters have also been used as starting free-ion parameters to optimize the energy level structure of Ln³⁺:elpasolite³⁰ and ODA (Ref. 31) systems. In some other cases, the influence of free-ion parameters have been ignored [for example, Ln³⁺:LnMO₄ (Ln = Gd, Y, Lu, and M=P, As,V)].³² In the CF analysis for Ln³⁺:elpasolites, not all free-ion values are varied if observed energy levels are few in number. In those cases, only F^2 are varied by fixing F^4 and F^6 with a hydrogenic ratios.³³

TABLE II. Experimental (E_{exp}) and calculated (E_{cal}) energy levels for the Nd³⁺-doped BGO. All values are in cm⁻¹.

Level ^a	$E_{\text{exp}}^{\text{b}}$	$E_{\text{cal}}^{\text{c}}$	ΔE^{d}
$^4I_{9/2}$	0	-17	17
	50	77	-27
	95	141	-46
	365	363	2
	444	472	-28
$^4I_{11/2}$	1920	1884	36
	1931	1923	8
	1956	1957	-1
	(2178) ^e	2103	75
	2195	2200	-5
$^4I_{13/2}$	2207	2238	-31
	(3870)	3820	50
	3875	3853	22
	3887	3880	7
		4011	
$^4I_{15/2}$	4153	4129	24
	4175	4185	-10
	4200	4219	-19
	5790	5777	13
	5804	5809	-5
$^4F_{3/2}$	5840	5851	-11
	(5885)	6025	140
	6195	6168	27
	6275	6243	32
	6303	6297	6
$^4F_{5/2}$	6333	6332	1
	(11327)	11392	-65
$^4F_{7/2}$	11460	11495	-35
	12329	12313	16
$^2H(2)_{9/2}$		12361	
	12418	12412	6
$^2H(2)_{9/2}$		12487	
	12516	12496	20
$^4F_{5/2}$		12546	
	12632	12600	32
$^2H(2)_{9/2}$	12676	12667	9
	13286	13276	10
$^4F_{7/2}$		13328	
	(13423)	13373	50
	13459	13458	1
$^4S_{3/2}$	13481	13463	18
	13492	13486	6

TABLE II. (*Continued.*)

Level ^a	$E_{\text{exp}}^{\text{b}}$	$E_{\text{cal}}^{\text{c}}$	ΔE^{d}
$^4F_{9/2}$		14519	
	14571	14586	-15
	14670	14677	-7
	14806	14827	-21
	14855	14839	16
$^2H(2)_{11/2}$	(15805)	15860	-55
	15833	15868	-35
	15848	15875	-27
		15951	
	15997	15973	24
$^4G_{7/2}$	16032	15982	50
		16658	
		16710	
		16718	
	16798	16791	7
$^4G_{5/2}$	16960	16934	26
	(17058)		
	17164	17160	4
	(17265)		
	(17290)		
$^4G_{7/2}$	17409	17414	-5
		18624	
		18676	
	18719	18770	-51
	(18836)		
$^4G_{9/2}$	18886	18883	3
	(18966)	19152	-186
	19168	19163	5
		19190	
		19296	
$^2K_{13/2}$	19338	19307	31
	(19457)		
	19492	19534	-42
	19588		
	(19708)	19641	67
$^2G(1)_{9/2}$	19802	19821	-19
	(20016)	20085	-69
		20129	
		20170	
		20452	
$^4G_{11/2}$		20454	
		20591	
		20685	
	20764	20771	-7
	21035	21024	11

TABLE II. (Continued.)

Level ^a	$E_{\text{exp}}^{\text{b}}$	$E_{\text{cal}}^{\text{c}}$	ΔE^{d}
	21065	21083	-18
	21189	21188	1
		21554	
² K _{15/2}	21577	21560	17
		21600	
		21681	
⁴ G _{11/2}		21695	
		21725	
² K _{15/2}		21852	
		21940	
² D _{3/2}		22064	
		22134	
² K _{15/2}		22151	
		22200	
		22218	
² D _{5/2}	23132	23165	-33
		23340	
		23476	
² P _{1/2}		24303	

^aIdentified by principal SLJ (multiplet) parentage.

^bFrom Ref. 17.

^cObtained using the parameters given in Table I for Nd³⁺-doped BGO.

^d $\Delta E = E_{\text{exp}} - E_{\text{cal}}$.

^eValues shown in parentheses were left out in fitting.

All of the above facts indicate that either ignoring or considering a different set of free-ion parameters while performing crystal-field analysis may not greatly distort the crystal-field parameters.

It is also noticed that, in general, only F^k and ξ and in some cases α , β and γ are allowed to vary for energy level calculations.³³ Though the T^i , M^j , and P^k are considered as variables in the H_{FI} , fixed values are used in most of the work. In our earlier work, varying T^i , M^j , and P^k did not change either of the trends in CF parameter values or any improvement in the σ value but did result in inconsistent values of T^i , M^j , and P^k .³³

In the case of CF analysis, if CF parameters are available for any of lanthanide-doped BGO or BSO, then those CF parameters may be used as starting CF parameters for other CF analysis involving these systems. If CF parameters are not available then it is always better to start a CF analysis with Eu:BGO or BSO systems, due to its characteristic energy level structure, as described elsewhere.³⁴ Of course, in some cases, the starting CF parameters may be theoretical ones obtained by various ways, e.g., *ab initio* or point-charge model.

In the present work, the CF analysis for Eu³⁺:BGO has been carried as follows. Initially, second rank CF parameters

TABLE III. Experimental (E_{exp}) and calculated (E_{cal}) energy levels for the Nd³⁺-doped BSO system. All values are in cm⁻¹.

Level ^a	$E_{\text{exp}}^{\text{b}}$	$E_{\text{cal}}^{\text{c}}$	ΔE^{a}
⁴ I _{9/2}	0	9	-9
	47	88	-41
	60	116	-56
	360	329	31
	450	489	-39
⁴ I _{11/2}	1915	1896	19
	1928	1926	2
	1954	1955	-1
	2182	2086	96
	2195	2198	-3
	2209	2239	-30
⁴ I _{13/2}	3860	3834	26
	3868	3860	8
	3880	3878	2
		3995	
	4152	4122	30
	4173	4184	-11
	4200	4218	-18
⁴ I _{15/2}	5823	5793	30
	5842	5819	23
	5870	5854	16
	5925	5992	-67
	6212	6169	43
	6271	6245	26
	6302	6296	6
	6332	6329	3
⁴ F _{3/2}	11336	11395	-59
	11472	11498	-26

^aSee footnote a and d of Table II.

^bFrom Ref. 17.

^cObtained using the parameters given in Table I for Nd³⁺-doped BSO.

were optimized and fixed with the help of Stark splittings of ⁷F₁ of Eu:BGO. Further optimization of second rank and fixing of fourth rank CF parameters were carried out with the help of ⁷F₁ and ⁷F₂ Stark levels. Similarly further optimization of second and fourth and fixing of sixth rank CF parameters were carried out by considering the Stark levels of ⁷F₁, ⁷F₂, and ⁷F₃. All of these CF parameters have been further optimized with the help of ⁷F₀, ⁷F₁, ⁷F₂, ⁷F₃, ⁵D₀, ⁵D₁, ⁵D₂, and ⁵D₃ Stark levels and finally by considering all the 35 Stark levels of Eu:BGO. The CF parameters obtained (optimized) for Eu:BGO were used as starting CF parameters to optimize CF parameters for Nd:BGO, Nd:BSO, and Er:BGO systems.

The energy level analysis was carried out by using the complete $4f^m$ basis set for Nd³⁺ and Er³⁺ ions, whereas in the case of Eu³⁺ ions, the method employed in earlier studies¹⁹

TABLE IV. Experimental ($E_{\text{exp.}}$) and calculated ($E_{\text{cal.}}$) energy levels for the Eu^{3+} -doped BGO system. All values are in cm^{-1} .

Level ^a	$E_{\text{exp.}}^{\text{b}}$	$E_{\text{cal.}}^{\text{c}}$	ΔE^{a}
7F_0	0	-9	9
7F_1	(240) ^a	320	-80
	439	473	-34
7F_2	890	886	4
	980	1034	-54
	1195	1186	9
7F_3	1826	1822	4
	1916	1908	8
	1933	1966	-33
	1977	1973	4
	2050	2027	23
7F_4		2689	
		2798	
	(3029)	2856	173
	(3065)	2900	165
	3094	3095	-1
	3115	3123	-8
7F_5	3783	3804	-21
	3818	3815	3
		3858	
	3894	3913	-19
	4001	4032	-31
	4076		
7F_6	4820	4885	-65
		4882	
	4927	4946	-19
		4993	
		5173	
		5217	
		5268	
		5310	
	5319	5315	4
5D_0	17256	17260	-4
5D_1	18983	18992	-9
	19024	19038	-14
5D_2	21425	21452	-27
	21451	21499	-48
	21546	21519	27
5D_3		24374	
	24376	24380	-4
	(24759)	24404	355
	(24815)	24424	391
	(24877)	24428	449

TABLE IV. (*Continued.*)

Level ^a	$E_{\text{exp.}}^{\text{b}}$	$E_{\text{cal.}}^{\text{c}}$	ΔE^{a}	
5L_6		24950		
		24970		
		25018		
		25042	25038	4
			25234	
		25353	25377	-24
5L_7		25417	25404	13
		25441	25461	-20
			25480	
			26040	
			26054	
		26069	26069	0
5G_2		26114	26074	40
		(26204)		
		26276	26278	-2
			26304	
5D_4		26357	26364	-7
			26384	
5D_4		(27552)		
		(27581)		
		(27601)		
		27629	27657	-28
			27661	
		27679		

^aSee footnote a, d, and e of Table II.

^bFrom Ref. 18.

^cObtained using the parameters given in Table I for Eu^{3+} -doped BGO.

was adopted to reduce the size of the matrix. First, the free-ion Hamiltonian was diagonalized within the entire $4f^6$ configuration. The resulting eigenvectors were used to transform both the crystal-field and free-ion matrix elements into an intermediate-coupling basis set. A relatively small basis set, truncated to a few thousand wave numbers above the highest observed levels, was then used in the parameter fit.^{23,33,35}

Standard least-square methods were used in a semiempirical fitting approach for the $4f^n$ -electronic structure problem²¹ and the fitting process minimizes the σ value. The CF strength (S) defined by Chang *et al.*²⁹ was used and it derived the S value that provides a measure for comparing the crystal-field strengths of different compounds on the rare earth ion.

The empirical databases available for the present systems were not large enough to support an analysis in which all 20 free-ion energy parameters could be treated as freely varying fitting parameters. The T^i , M^j , and P^k parameters were assigned fixed values in the energy level fitting procedures. The P^4 , P^6 , M^2 , and M^4 parameters were constrained according to $P^4=0.75P^2$, $P^6=0.50P^2$, $M^2=0.56M^0$, and $M^4=0.38M^0$. The values taken for these fixed parameters were

those obtained from an analysis of Ln³⁺-doped LaCl₃.³⁵ In the present work, a well optimized set of free-ion parameters as derived from the highly reliable energy level scheme of Ln³⁺:LaCl₃ (Ref. 35) was used as the starting free-ion parameters for CF analysis.^{30,31,33} Calculations performed on the Nd³⁺ and Er³⁺ systems were carried out by diagonalizing the total (atomic and crystal-field) Hamiltonian within the complete 364 JM_J states. In the case of Eu³⁺-doped BGO, a basis set of 488 JM_J states comprising 50 SLJ multiplets, which covers up to 41 000 cm⁻¹, was used in the crystal-field calculations.

D. Radiative properties and Judd-Ofelt analysis

In order to quantitatively estimate the radiative spectral properties of Nd³⁺, the absorption band line strengths (S_{exp}) were evaluated using a standard procedure.¹ The experimental line strengths were then fitted with theoretical line strength (S_{cal}) following the Judd-Ofelt procedure.^{36,37} The three Judd-Ofelt parameters (Ω_2 , Ω_4 , and Ω_6) were obtained by fitting the measured oscillator strength to the theoretical oscillator strength using a least-squares method. Judd-Ofelt parameters can be used to calculate the radiative transition probability (A_{rad}) between the excited states. The radiative lifetime of an emitting state is related to the total spontaneous emission probability of all the transitions from an excited state by $\tau_{\text{RAD}} = (\sum A_{\text{rad}})^{-1}$ and the luminescence branching ratio of a transition is obtained from the expression $\beta_{J'J} = A_{\text{rad}} \tau_{\text{RAD}}$. The stimulated emission cross section of the emission band is obtained with the Fuchtbauer-Ladenburg equation.¹ The quality of the fit in the Judd-Ofelt approximation is obtained by minimizing the σ value between the experimental and theoretical line strength.

III. RESULTS AND DISCUSSION

A. Energy levels and crystal field analysis

For Nd³⁺-doped BSO and Er³⁺-doped BGO, empirical energy level data at 77 K reported by Kaminiskii *et al.*¹⁷ were used. Tsuboi *et al.*¹⁸ reported the energy level structure for Eu³⁺-doped BGO from optical absorption and luminescence studies at 10 K. These data were taken without any reassignment and were fitted using Eq. (1). The atomic and crystal-field parameters for Ln³⁺-doped BGO (Ln = Nd, Eu, and Er) and Nd³⁺-doped BSO obtained from the systematic model Hamiltonian and also experimental and calculated energies are presented in Tables I–VI. Table I shows the energy parameters obtained for the complete set of observed energy levels listed in Tables II–V for Nd³⁺-doped BGO, Nd³⁺-doped BSO, Eu³⁺-doped BGO, and Er³⁺-doped BGO, respectively. Some of the energy levels under the E_{exp} column are shown in parentheses, as these levels were not considered while fitting the data. An inclusion of these levels in the fit leads to larger σ values.

Here the energy parameters are obtained by considering all the observed levels for each data set ignoring few levels,

TABLE V. Experimental (E_{exp}) and calculated (E_{cal}) energy levels for the Er³⁺-doped BGO system. All values are in cm⁻¹.

Level ^a	E_{exp} ^b	E_{cal} ^c	ΔE^a
⁴ I _{15/2}	10	39	-29
	46	68	-22
	74	105	-31
	(380) ^a	236	144
	385	397	-12
	402	417	-15
⁴ I _{13/2}	412	439	-27
	6493	6492	1
	6532	6514	18
	6558	6546	12
	(6573)	6634	-61
	6783	6765	18
	6788	6773	15
	6795	6793	2
⁴ I _{11/2}	10173	10180	-7
	10213	10196	17
	10230	10242	-12
	10323	10321	2
	10326	10326	0
	10334	10335	-1
⁴ I _{9/2}	12344	12332	12
	12414	12409	5
	12513	12526	-13
	12577	12576	1
	12609	12609	0
⁴ F _{9/2}	15141	15144	-3
	15163	15174	-11
	15264	15261	3
	15348	15324	24
⁴ S _{3/2}	15394	15402	-8
	18280	18282	-2
	18354	18336	18
² H _{11/2}		19075	

TABLE V. (Continued.)

Level ^a	E_{exp}^b	$E_{\text{cal.}}^c$	ΔE^a
		19087	
		19105	
		19206	
		19250	
		19262	

^aSee footnote a, d, and e of Table II.

^bFrom Ref. 17.

^cObtained using the parameters given in Table I for Er³⁺-doped BGO.

which differ considerably from calculated values. Out of 70 levels observed for Nd³⁺-doped BGO, only 56 levels were considered for the fit, which yields a σ value of $\pm 22 \text{ cm}^{-1}$ (Table I). If we include all 70 observed levels, σ was found to be $\pm 85 \text{ cm}^{-1}$ with a different set of energy parameter values. In the case of Nd³⁺-doped BSO data, all the observed 27 levels were considered and the fit produced a σ value of $\pm 41 \text{ cm}^{-1}$. As seen from Table III, the levels of 60, 2182, 5925, and 11336 cm^{-1} fit with a large deviation. The energy levels for Eu³⁺-doped BGO were analyzed with an rms deviation of $\pm 22 \text{ cm}^{-1}$ for 35 levels (Table IV). Table V shows the experimental and calculated values for Er³⁺-doped BGO. For this system, the fit gives a $\sigma = \pm 16 \text{ cm}^{-1}$ for 31 levels and better agreement between the calculated and observed crystal-field splitting. The crystal-field parameters used by

TABLE VI. Comparison of crystal-field parameters determined with all multiplets and common multiplets for the Nd³⁺ system. The free-ion parameters for the calculations are taken from Table I for respective systems and are fixed. Column 2 refers to the B_q^k parameters obtained from the fit for 56 observed levels (column 2 of Table I). Columns I (G) and I (S) refer to the B_q^k parameters obtained from the fit for common crystal-field levels spanning the lowest 5 multiplets. Columns II (G) and II (S) refer to the B_q^k parameters obtained after deleting three levels, which gives major discrepancy with calculated values. For definitions of N , σ , and S , see footnote of Table I.

Parameters	Nd:BGO	Nd:BGO	Nd:BSO	Nd:BGO	Nd:BSO
		I(G)	I(S)	II(G)	II(S)
E_{AVG}	24971	24963	24968	24972	24974
B_0^2	836	870	824	-51	-120
B_0^4	63	-61	-169	426	238
B_3^4	± 2220	± 1987	± 2067	± 2055	± 2012
B_0^6	147	310	335	141	212
B_3^6	± 90	± 50	± 42	± 136	± 26
B_6^6	423	630	468	714	707
N	56	27	27	24	24
σ	± 22	± 43	± 41	± 15	± 23
S	305	605	604	589	574

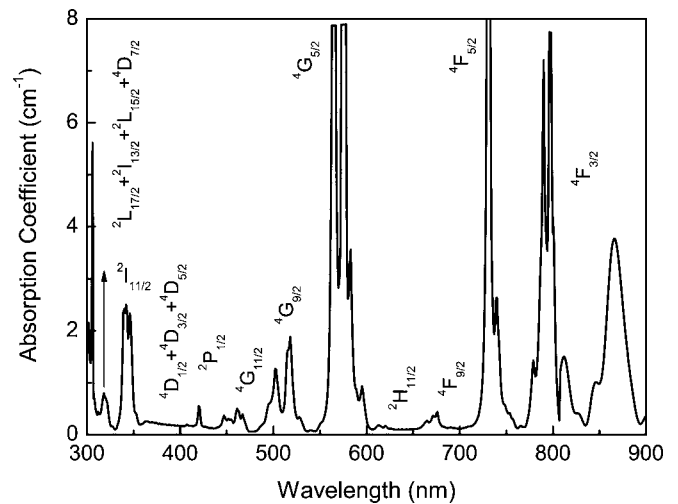


FIG. 2. Room temperature optical absorption spectrum of a Nd³⁺-doped BGO crystal. The Nd³⁺ dopant concentration is 2.2 wt. % which corresponds to an ionic concentration of $6.63 \times 10^{20} \text{ ions/cm}^3$.

Morrison and Leavitt¹⁹ differ somewhat from the parameters obtained in the present analysis. This is because their fitting analysis was carried out by ignoring T^i , M^j , and P^k parameters in the model Hamiltonian since few lowest multiplets were considered for the fit. Though they also considered imaginary crystal-field parameters in the crystal-field model Hamiltonian, the crystal-field strength (S) derived with and without imaginary terms was identical. For example, in the Er³⁺-doped BGO system¹⁹ an S value was found to be 524 cm^{-1} both with and without imaginary crystal-field parameters. In earlier crystal-field analysis for lanthanide ions, it was found that the energy parameters differ quantitatively due to differences in the Hamiltonian model where the data set used in the fit also differed.^{38,39} Therefore, in the present work, energy level analysis has been carried out using uniform model Hamiltonian as well as common multiplets that yield reasonably correct values of CF parameters. Table VI shows the crystal-field parameters obtained for Nd³⁺-doped BGO and Nd³⁺-doped BSO systems for the common multiplets.

Out of the assigned levels of the Nd³⁺-doped BGO and Nd³⁺-doped BSO, 27 have common assignments and may be compared on a level-to-level basis to provide a meaningful comparison of crystal-field and crystal-field strength parameters. The crystal-field parameters given in Table VI are listed as sets I (G)/II (G) and I (S)/II (S) for the Nd³⁺-doped BGO and Nd³⁺-doped BSO, respectively. Parameter sets II (G) and II (S) of Table VI were obtained analogously to sets I (G) and I (S), but the former sets were derived from 24 common levels and latter for 27. The three common energy levels that are deleted in II (B)/II (S) are 2178, 5885, and 11327 cm^{-1} for Nd³⁺-doped BGO and 2182, 5925, and 11336 cm^{-1} for Nd³⁺-doped BSO. Ignoring these levels in the fit, the σ value is reduced from ± 43 to ± 15 and ± 41 to $\pm 23 \text{ cm}^{-1}$, respectively, for Nd³⁺-doped BGO and BSO systems.

Focusing on the magnitude of the “ S ” value (Table I), we note that the Eu³⁺ ion experiences relatively larger crystal-

TABLE VII. Observed absorption bands along with the experimental and calculated line strengths ($\Omega_2 = 1.5 \times 10^{-20} \text{ cm}^2$, $\Omega_4 = 3.02 \times 10^{-20} \text{ cm}^2$, $\Omega_6 = 3.15 \times 10^{-20} \text{ cm}^2$, and $\sigma = 1.7 \times 10^{-20} \text{ cm}^2$) for the Nd:BGO.

Levels	Wavelength ^a (nm)	$\int \alpha(\lambda) d\lambda$ ^b (10 ⁻⁷)	S_{exp} (10 ⁻²⁰ cm ²)	S_{cal} (10 ⁻²⁰ cm ²)
${}^2L_{17/2} + {}^2I_{13/2} + {}^2L_{15/2} + {}^4D_{7/2}$	318	14.0	4.04	2.8
${}^2I_{11/2}$	342	29.77	8.0	6.0
${}^4D_{1/2} + {}^4D_{3/2} + {}^4D_{5/2}$	363	11.2	2.8	1.5
${}^2D(1)_{5/2} + {}^2P_{1/2}$	420	2.89	0.63	0.2
${}^2G(1)_{9/2} + {}^2K_{15/2} + {}^2D(1)_{3/2} + {}^4G_{11/2}$	462	10.43	2.07	0.9
${}^4G_{9/2} + {}^2K_{13/2} + {}^4G_{7/2}$	517	36.54	6.49	4.4
${}^2G_{7/2} + {}^4G_{5/2}$	575	152.9	24.44	23.0
${}^2H(2)_{11/2}$	615	3.08	0.45	0.3
${}^4F_{9/2}$	676	6.4	0.87	0.5
${}^4F_{5/2} + {}^2H(2)_{9/2}$	731	87.12	10.95	10.0
${}^4F_{3/2}$	800	110.03	12.34	11.8

^aInstrumental error in the wavelength measurement = ± 0.02 nm.

^bInstrumental error in the absorption coefficient (α) = $\pm 0.0001/\text{cm}$.

field strength than that of the Nd³⁺ ion in BGO. The Er³⁺ ion experiences a medium crystal-field strength. As seen from Table VI, the S value obtained for common levels of two different environments shown under I (G) and I (S) were found to be more or less similar but a slight difference was noticed between II (G) and II (S) sets of parameters. Also, the S value obtained for 56 levels is 305 cm^{-1} , which differs from the $S=605 \text{ cm}^{-1}$, obtained for 27 levels for the Nd³⁺-doped BGO system.

Comparing the CF parameters sets that are obtained for each system independently (Table I) as well as for common levels of Nd³⁺:BGO or BSO (Table VI), systematic trends are not noticed. This may be due to the fact that the small number of levels, used in the fit and also because most of the high energy levels are yet to be measured and the need to reconfirm the reported experimental values.¹⁷ Though the

crystal-field parametrization is phenomenological, which depends on the nature of data sets used for the analysis, the present energy level analysis provides the basis to identify and assign higher levels, which may be helpful for improving future energy level analysis for these materials. Therefore, speculations concerning the significance (and meaning) of these results are best deferred until more Stark levels and also similar findings for other systems are available.

B. Transition intensities and radiative properties

For the calculation of the transition intensities of various absorption bands, the room temperature absorption spectrum shown in Fig. 2 is employed. There are as many as 12 transitions corresponding to transitions from the ${}^4I_{9/2}$ ground state manifold to various excited states of the $4f^3$ -electronic configuration with weak Stark splitting for some of the tran-

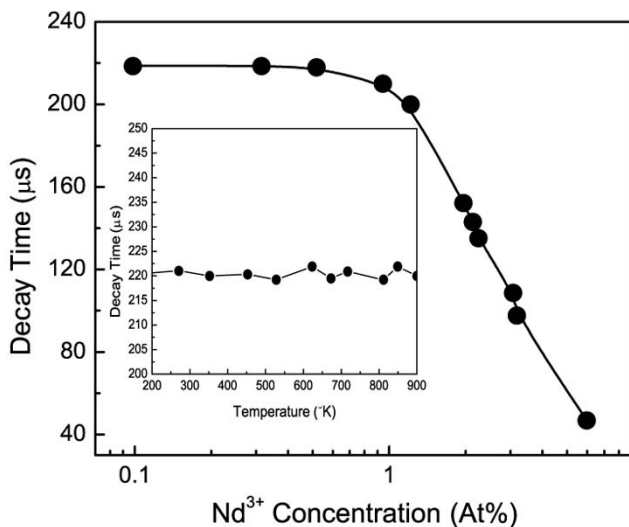


FIG. 3. Concentration dependence of the ${}^4F_{3/2}$ decay time of Nd³⁺ in a BGO crystal. The inset shows the temperature dependence of the fluorescence decay.

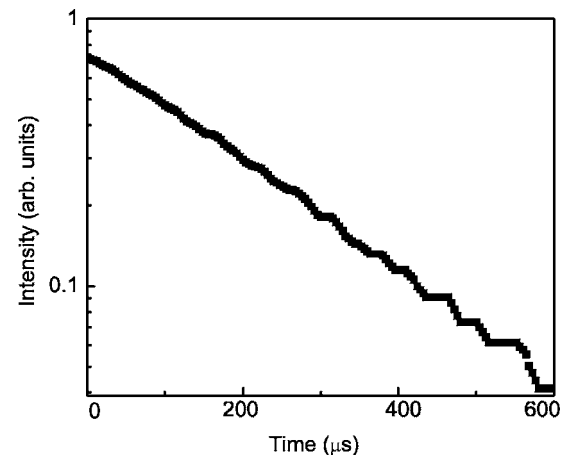


FIG. 4. Fluorescence decay curves of the 1064.4 nm emission band using 800 nm excitation for Nd³⁺:BGO. The Nd³⁺ concentration in the crystal is 6.63×10^{20} ions/cc.

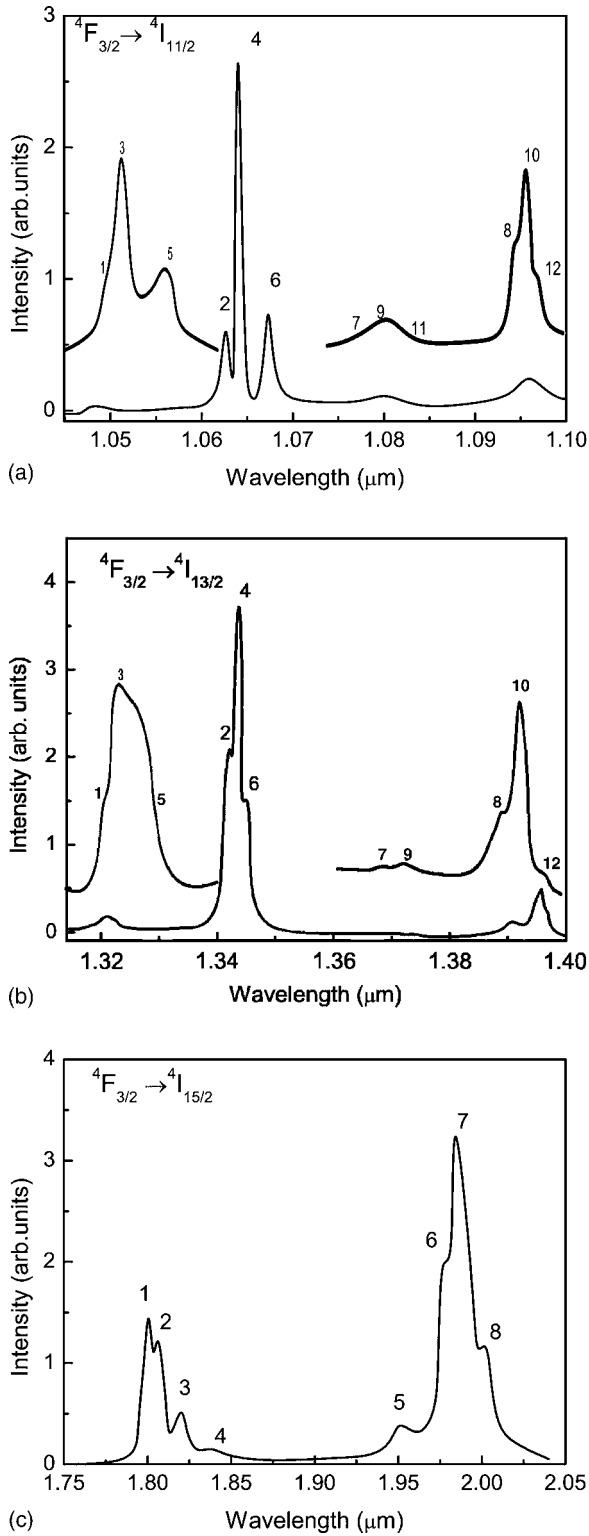


FIG. 5. Fluorescence spectra of Nd^{3+} ions in a BGO crystal at 77 K with corresponding Stark level notations for (a) ${}^4F_{3/2} \rightarrow {}^4I_{11/2}$, (b) ${}^4F_{3/2} \rightarrow {}^4I_{13/2}$, and (c) ${}^4F_{3/2} \rightarrow {}^4I_{15/2}$ transitions.

sitions. The centers of gravity of these manifolds are listed in Table VII along with their band assignments and measured electric dipole line strengths. The Judd-Ofelt parametrization^{36,37} yields the following values: $\Omega_2 = 1.5 \times 10^{-20} \text{ cm}^2$, $\Omega_4 = 3.02 \times 10^{-20} \text{ cm}^2$, and $\Omega_6 = 3.15$

TABLE VIII. Observed intermanifold transitions and their spectral characteristics for (a), (b), and (c) fluorescence transitions of Nd:BGO.

Line	λ_{ij} (μm)	β_{ij} (%)	$A_{ij}(\text{s}^{-1})$	$\Delta\nu$ (cm^{-1})	$\sigma_{e,ij}(10^{-19} \text{ cm}^2)^a$
(a) ${}^4F_{3/2} \rightarrow {}^4I_{11/2}$					
1	1.0482	0.22	130	9	0.026
3	1.0494	1.16	660	9	0.13
5	1.0522	1.04	590	12	0.09
2	1.0630	6.0	300	3	2.1
4	1.0642	24.0	1180	2.7	9.2
6	1.0671	9.4	465	4	2.4
7	1.0773	0.6	340	20	0.03
9	1.0793	0.85	480	20	0.05
11	1.0807	0.4	225	20	0.02
8	1.0930	3.0	150	13	0.26
10	1.090	6.15	350	13	0.5
12	1.0965	1.0	50	15	0.15
(b) ${}^4F_{3/2} \rightarrow {}^4I_{13/2}$					
1	1.3175	0.03	37	10	0.007
3	1.3184	0.15	188	10	0.05
5	1.3205	0.12	165	12	0.04
2	1.3410	1.8	73	4	0.64
4	1.3419	7.35	390	4	3.41
6	1.3441	1.50	49	5	0.34
7	1.3685	0.02	37	20	0.006
9	1.3729	0.03	57	20	0.009
8	1.3939	0.24	8	13	0.02
10	1.3984	0.54	19	15	0.04
12	1.4031	0.03	2	17	0.007
(c) ${}^4F_{3/2} \rightarrow {}^4I_{15/2}$					
1	1.8060	0.714	23	26	0.089
2	1.8106	0.617	19	31	0.074
3	1.8225	0.261	8	36	0.064
4	1.8375	0.077	2	29	0.078
5	1.9485	0.193	6	53	0.050
6	1.9790	0.998	32	33	0.083
7	1.9905	1.628	52	37	0.074
8	2.0024	0.581	18	26	0.10

^aEmission cross section for the intermanifold ($i \rightarrow j$) transitions.

$\times 10^{-20} \text{ cm}^2$ with a quality factor $\Omega_4/\Omega_6 = 0.95$. These results are in the range of reported values for other solid-state laser materials.¹ A large value of the quality factor is desirable since it determines the fluorescence branching ratio of the ${}^4F_{3/2}$ metastable manifold can be quantitatively studied. The ${}^4F_{3/2}$ excited state of Nd^{3+} decays into four emission channels. These are ${}^4F_{3/2} \rightarrow {}^4I_J$ ($J = \frac{9}{2}, \frac{11}{2}, \frac{13}{2}$, and $\frac{15}{2}$) with emission wavelengths corresponding to 920, 1064.4, 1341.8, and 1990.5 nm, respectively. The experimentally measured fluorescence branching ratios are on the order $\beta_{11/2} > \beta_{13/2} > \beta_{15/2} > \beta_{9/2}$. In order to measure the ra-

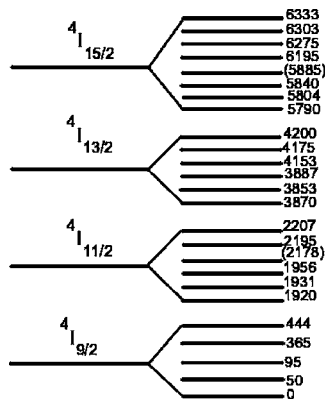


FIG. 6. Observed low temperature Stark level splitting of the 4I_J manifolds of Nd³⁺ ions in a BGO crystal. The energy values are in cm⁻¹. The bands in parentheses are not observed.

diative quantum efficiency of the ${}^4F_{3/2}$ decay, the measured luminescence decay time, τ_{LUM} is connected with the sum of radiative (A_{rad}) and temperature dependent nonradiative ($d_{ij}[T]$) transitions. Using the above relationship, quantum efficiency of the emission can be determined, provided the concentration and temperature dependence of τ_{LUM} is known. The quantum efficiency is estimated as the ratio of the radiative decay rate to the sum of radiative plus nonradiative decay rates.¹

The temperature and concentration dependence of the ${}^4F_{3/2}$ decay time is shown in Fig. 3. The constant value of the lifetime with temperature up to 900 K indicates that the deactivation of the ${}^4F_{3/2}$ metastable level is mainly controlled by the radiative transitions, i.e., $d_{ij} \ll A_{\text{rad}}$ and $\eta=1$ (i.e., 100% quantum efficiency). The decay curve of the ${}^4F_{3/2} \rightarrow {}^4I_{11/2}$ bands at 2.2 wt. % Nd concentration is shown in Fig. 4. An exponential fitting of the decay curve yields a decay time of 220 μs . The measured lifetimes are in agreement with the reported lifetime of Nd³⁺ in many other solid-state laser materials.¹

C. Stark level analysis

A detailed analysis of the various Stark levels in the emission spectrum of Nd³⁺ in BGO permits us to quantitatively identify the stimulated emission channels possible in this system. Using the low temperature absorption and emission data, the Stark splitting of the various observed absorption bands and their stimulated emission characteristics could be evaluated. For a rare earth ion like Nd³⁺, there can be many crystal-field levels both in absorption and emission spectra and hence the transition probability (A_{ij}) of a particular Stark level should be evaluated by considering the Boltzmann's factor of that level using a standard procedure.¹ Using these inter-Stark transition probabilities one can evaluate the corresponding stimulated emission cross section for the inter-Stark transition ($\sigma_{e,ij}$).

A typical low temperature fluorescence spectrum recorded for the 2.2 at. % Nd³⁺ ion is shown in Fig. 5. For the ${}^4F_{3/2} \rightarrow {}^4I_{11/2}$ and ${}^4I_{13/2}$ transitions 12 and 11 Stark levels, respectively, were observed in the spectrum. In contrast, for the

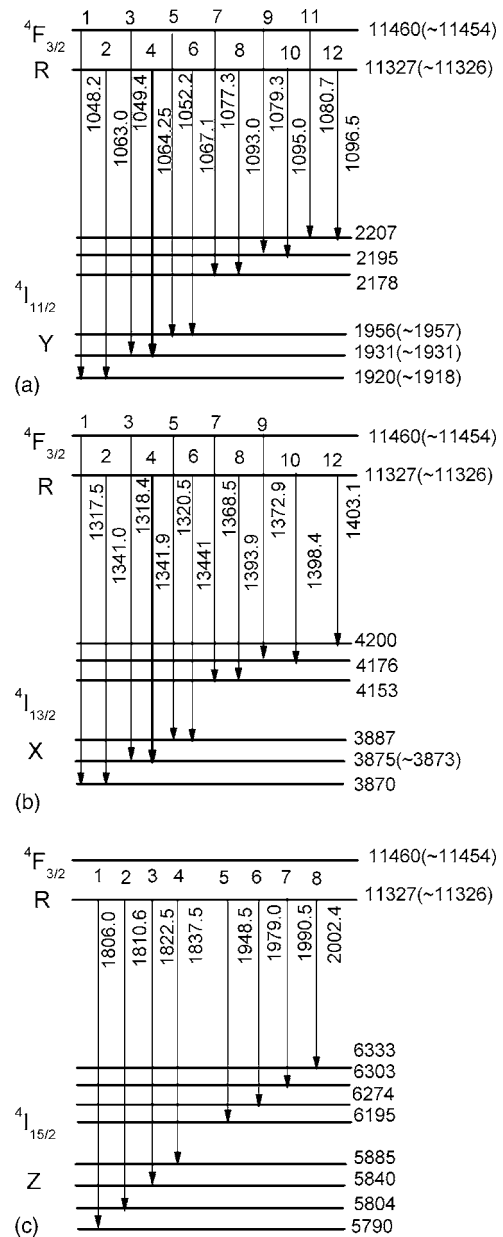


FIG. 7. Stark level splitting scheme and observed intermanifold transitions of Nd³⁺ ions in a BGO crystal for (a) ${}^4F_{3/2} \rightarrow {}^4I_{11/2}$, (b) ${}^4F_{3/2} \rightarrow {}^4I_{13/2}$, and (c) ${}^4F_{3/2} \rightarrow {}^4I_{15/2}$ transitions with corresponding band positions. The transition wavelengths are in nm and the energies of the levels are in cm⁻¹. The values in parentheses are for room temperature.

${}^4I_{15/2}$ band, 8 Stark levels were observed. The inter-Stark branching ratio (β_{ij}) was obtained by multiplying the relative spectral emission density of each line with the total branching ratio of the emission band. The inter-Stark branching ratio was then used for the computation of the various Stark levels transition probability. The calculated inter-Stark fluorescence branching ratio, transition probability, spectral bandwidth ($\Delta\lambda$), and stimulated emission cross sections are summarized in Table VIII for the three observed emission bands.

The energy level diagram can be deduced from the observed emission spectra. The observed fluorescence levels

TABLE IX. Summary of the spectral characteristics of the ${}^4F_{3/2} \rightarrow {}^4I_{11/2}$ and ${}^4F_{3/2} \rightarrow {}^4I_{13/2}$ bands at room temperature and low temperature of Nd:BGO.

Characteristics	77 K	300 K			
	${}^4F_{3/2} \rightarrow {}^4I_{11/2}$	${}^4F_{3/2} \rightarrow {}^4I_{11/2}$			${}^4F_{3/2} \rightarrow {}^4I_{13/2}$
		$R_1 \rightarrow Y_1$	$R_1 \rightarrow Y_1$	$R_1 \rightarrow Y_2$	$R_1 \rightarrow Y_3$
Wavelength (λ nm)	1064.25	1063	1064.4	1067.1	1341.8
Refractive index (n)	2.04	2.04	2.04	2.04	2.0
Fluorescence branching ratio (β_{ij} %)	26	4.3	17	6.7	6.9
Radiative transition probability (A_{ij} s $^{-1}$)	1190	300	1180	465	480
Emission cross section ($\sigma_{e,ij} 10^{-19}$ cm 2)	9.2	0.3	1.1	0.3	1.0
$\Delta\nu_{ij}$ (cm $^{-1}$)	3	23	24	36	29

are shown in Fig. 6. The observed Stark levels are schematically shown in the energy level diagrams (Fig. 7) following the notation of Dieke.^{40,41} With the spectral characteristics summarized in Table IX, the effective stimulated emission cross section (σ_e^{eff})¹ of the ${}^4F_{3/2} \rightarrow {}^4I_{11/2}$ channel at 300 K is obtained as 1.34×10^{-19} cm 2 . This value is nearly six times lower than that of the widely used Nd $^{3+}$ -doped yttrium aluminum garnet crystal ($\sigma_e^{\text{eff}} \sim 7.7 \times 10^{-19}$ cm 2) with $\lambda = 1064.15$ nm at 300 K.⁴² In a similar way, the effective stimulated emission cross section of the ${}^4F_{3/2} \rightarrow {}^4I_{13/2}$ transition is estimated to be 1.0×10^{-19} cm 2 . Even though the high value of the stimulated emission cross section can contribute to the high gain of the emission channel, it also shows that in some cases large values of the stimulated emission cross section are not necessary for devices with high output characteristics.⁴³ For example, in Q -switched lasers, because of the high σ_e^{eff} value, there may be the chances of intensive superluminescence, which will lead to the limitation of the population of the ${}^4F_{3/2}$ metastable level. In such lasers, the most active media are those with σ_e^{eff} of the order of $1-1.5 \times 10^{-19}$ cm 2 at 300 K. For Nd:BGO the σ_e^{eff} of both ${}^4F_{3/2} \rightarrow {}^4I_{11/2}$ and ${}^4F_{3/2} \rightarrow {}^4I_{13/2}$ transitions are in the same range, which enables its possible application for Q -switched lasers.

IV. CONCLUSIONS

Nd $^{3+}$ -doped BGO single crystals were grown by the modified Czochralski method. A detailed spectroscopic study was done on the energy level structure and radiative spectral properties at room temperature as well as low temperature. It was established through absorption and emission measurements that the spectral properties are very similar to earlier reported data. A systematic crystal-field analysis for the Ln $^{3+}$:BGO (Ln = Nd, Eu, and Er) and Nd $^{3+}$:BSO systems have been carried out using C_{3v} point symmetry. The importance and reliability of these derived crystal-field parameters

by assuming low symmetry is in accordance with the reliability and compatibility that were well documented by earlier reports. Though our energy levels are not sufficient for crystal-field analysis, the present energy level scheme shows that Eu $^{3+}$ ion experiences a relatively larger crystal-field strength than that of Nd $^{3+}$ ion in BGO, whereas the Er $^{3+}$ ion experiences a medium crystal-field strength. The radiative lifetime for ${}^4F_{3/2}$ remains constant up to 900 K, which indicates the absence of nonradiative deactivation for this level. For Nd $^{3+}$ ion concentrations up to 0.5 at. %, the decay curve for the ${}^4F_{3/2}$ level was found to be a single exponential, which indicates that there is no nonradiative energy transfer between the emitting ions. The absence of nonradiative relaxation and energy transfer yields 100% quantum efficiency for the ${}^4F_{3/2}$ emission channel. From emission measurements as well as with the help of Judd-Ofelt theory, inter-Stark fluorescence branching ratios, transition probabilities, spectral bandwidths, and stimulated emission cross sections are presented for ${}^4F_{3/2} \rightarrow {}^4I_J$ ($J = \frac{11}{2}$ and $\frac{13}{2}$) and are comparable to the earlier reported values. The effective stimulated emission cross section of the principal emission band is observed to be nearly six times lower than that of the well-known laser host Nd:YAG, which enables its possible application for making Q -switched lasers.

ACKNOWLEDGMENTS

G.A.K. and R.E.R. acknowledge the support of the New Jersey Commission on Science and Technology, the Office of Naval Research and the U.S. Army through the South Carolina Research Authority (sub-recipient agreement 2001-509, task order 0007, *Active Coatings Technology* program. A.A.K. was supported by the Russian Academy of Sciences and the Russian Foundation for Basic Research. C.K.J. is grateful to DAE-BRNS, Government of India (Sanction No. 2003/34/4-BRNS/600, dt. 11.07.2003) for financial support.

*Corresponding author. Email address: akgsh@yahoo.com

- ¹A. A. Kaminski, *Laser Crystals-Their Physics and Properties* (Springer, Berlin, 1989).
- ²V. Y. Ivanov, A. V. Kruzhalov, Y. F. Kargin, V. A. Pustovarov, V. M. Skorikov, Y. A. Shumilov, and B. V. Shul'gin, *Sov. Phys. Solid State* **28**, 833 (1986).
- ³K. Okajima, K. Takami, K. Veda, and F. Kawaguchi, *Rev. Sci. Instrum.* **53**, 1285 (1982).
- ⁴V. Y. Ivanov, A. V. Kruzhalov, V. A. Pustovarov, and U. L. Petrov, *Nucl. Instrum. Methods Phys. Res. A* **261**, 150 (1987).
- ⁵*Handbook of Lasers*, edited by R. Pressley (CRC Press, Cleveland, 1971).
- ⁶S. K. Dickinson, R. M. Hilton, and H. G. Lipson, *Mater. Res. Bull.* **7**, 181 (1972).
- ⁷F. J. Lopez, E. Moya, and C. Zaldo, *Solid State Commun.* **76**, 1169 (1990).
- ⁸A. A. Kaminskii, S. E. Sakisov, T. I. Butaeva, G. A. Danisenko, B. Hermoneit, J. Bohm, W. Grosskerez, and D. Schulze, *Phys. Status Solidi A* **56**, 725 (1979).
- ⁹D. J. Segal, R. P. Santoro, and R. E. Newnham, *Z. Kristallogr.* **123**, 73 (1966).
- ¹⁰G. A. Kumar, R. E. Riman, S. C. Chae, Y. N. Jang, I. K. Bae, and H. S. Moon, *J. Appl. Phys.* **95**, 3243 (2004).
- ¹¹Y. N. Jang, N. H. Sung, S. C. Chae, I. K. Bae, and I. J. Kim, *Korean J. Crystallogr.* **8**, 38 (1997).
- ¹²J. B. Gruber, D. K. Sardar, R. M. Yow, T. H. Allik, and B. Zandi, *J. Appl. Phys.* **96**, 3050 (2004).
- ¹³G. W. Burdick, C. K. Jayasankar, F. S. Richardson, and M. F. Reid, *Phys. Rev. B* **50**, 16309 (1994).
- ¹⁴B. G. Wybourne, *Spectroscopic Properties of Rare Earths* (Academic, New York, 1965).
- ¹⁵D. Bravo and F. J. Lopez, *J. Chem. Phys.* **99**, 4952 (1993).
- ¹⁶A. A. Kaminskii, D. Schultze, B. Hermoneit, S. E. Sarkisov, L. Li, J. Bohm, P. Reiche, R. Ehlert, A. A. Mayer, V. A. Lomonov, and V. A. Balashov, *Phys. Status Solidi A* **88**, 737 (1976).
- ¹⁷A. A. Kaminskii, S. N. Bagayev, N. V. Kravtsov, S. N. Chekina, Ya. V. Vasiliev, N. I. Ivannikova, K. Ueda, J. Lu, H. J. Eichler, G. M. A. Gad, J. Hanuza, J. Fernandez, and P. Reiche, *Laser Phys.* **11**, 897 (2001).
- ¹⁸T. Tsuboi, H. J. Seo, B. K. Moon, and J. H. Kim, *Physica B* **270**, 45 (1999).
- ¹⁹C. A. Morrison and R. P. Leavitt, *J. Chem. Phys.* **74**, 25 (1981).
- ²⁰C. Rudowicz and J. Qin, *Phys. Rev. B* **67**, 174420 (2003).
- ²¹M. F. Reid (private communication).
- ²²G. W. Burdick and M. F. Reid, *Mol. Phys.* **102**, 1141 (2004).
- ²³W. T. Carnall, G. L. Goodman, K. Rajnak, and R. S. Rana, *J. Chem. Phys.* **90**, 3443 (1989).
- ²⁴C. K. Jayasankar and F. S. Richardson, *Phys. Status Solidi B* **155**, 221 (1989).
- ²⁵P. Porcher, D. R. Svoronos, M. Leskela, and J. Holsa, *J. Solid State Chem.* **46**, 101 (1983).
- ²⁶C. Rudowicz, *Chem. Phys.* **97**, 43 (1985).
- ²⁷C. Rudowicz and J. Qin, *J. Alloys Compd.* **385**, 238 (2004).
- ²⁸C. Rudowicz and J. Qin, *J. Lumin.* **110**, 39 (2004).
- ²⁹N. C. Chang, J. B. Gruber, R. P. Leavitt, and C. A. Morrison, *J. Chem. Phys.* **76**, 3877 (1982).
- ³⁰M. F. Reid and F. S. Richardson, *J. Chem. Phys.* **83**, 3831 (1985).
- ³¹D. M. Moran, Anne De Piante, and F. S. Richardson, *Phys. Rev. B* **42**, 3317 (1990).
- ³²C. Linares, A. Louat, and M. Blanchard, *Struct. Bonding (Berlin)* **33**, 179 (1977).
- ³³P. A. Tanner, V. V. Ravi Kanth Kumar, C. K. Jayasankar, and M. F. Reid, *J. Alloys Compd.* **215**, 349 (1994).
- ³⁴C. Cascales, E. Antic-Fidancev, M. Lemaitre-Blaise, and P. Porcher, *J. Solid State Chem.* **89**, 118 (1990).
- ³⁵C. K. Jayasankar, F. S. Richardson, and M. F. Reid, *J. Less-Common Met.* **148**, 289 (1989).
- ³⁶B. R. Judd, *Phys. Rev.* **127**, 750 (1962).
- ³⁷G. S. Ofelt, *J. Chem. Phys.* **37**, 511 (1962).
- ³⁸E. Rukmini, C. K. Jayasankar, and M. F. Reid, *J. Phys.: Condens. Matter* **6**, 5919 (1994).
- ³⁹A. Rukmini Devi, C. K. Jayasankar, and M. F. Reid, *J. Alloys Compd.* **207/208**, 74 (1994).
- ⁴⁰G. H. Dieke, *Spectra and Energy Levels of Rare Earth Ions in Crystals* (Wiley Interscience, New York, 1968).
- ⁴¹S. Singh, R. G. Smith, and L. G. Van Uitert, *Phys. Rev. B* **10**, 2566 (1974).
- ⁴²A. A. Kaminskii, *Laserniye Kristally* (Nauka, Moscow, 1975).
- ⁴³L. A. Riseberg, R. M. Brown, and W. C. Hilton, *Appl. Phys. Lett.* **23**, 127 (1973).